Enhancement of Novel View Synthesis Using Omnidirectional Image Completion

Takayuki Hara The University of Tokyo

hara@mi.t.u-tokyo.ac.jp

Tatsuya Harada The University of Tokyo / RIKEN

harada@mi.t.u-tokyo.ac.jp

Abstract

In this study, we present a method for synthesizing novel views from a single 360-degree RGB-D image based on the neural radiance field (NeRF). Prior studies relied on the neighborhood interpolation capability of multi-layer perceptrons to complete missing regions caused by occlusion and zooming, which leads to artifacts. In the method proposed in this study, the input image is reprojected to 360degree RGB images at other camera positions, the missing regions of the reprojected images are completed by a 2D image generative model, and the completed images are utilized to train the NeRF. Because multiple completed images contain inconsistencies in 3D, we introduce a method to learn the NeRF model using a subset of completed images that cover the target scene with less overlap of completed regions. The selection of such a subset of images can be attributed to the maximum weight independent set problem, which is solved through simulated annealing. Experiments demonstrated that the proposed method can synthesize plausible novel views while preserving the features of the scene for both artificial and real-world data.

1. Introduction

The synthesis of novel views from a set of captured images has a wide range of application, including AR/VR and immersive 3D photography. Conventionally, structure-from-motion [26] and image-based rendering [60] have been employed for this task. In recent years, neural networks-based rendering methods have been rapidly developed, and the neural radiance field (NeRF) [48] is a promising method for synthesizing photorealistic views. However, NeRF requires tens to hundreds of images with known relative positions and the same shooting conditions to be given as the input, and it is a large and time-consuming process. Accordingly, various efforts have been made to reduce the number of input images [79, 74, 72, 31] or ease the shooting conditions [47, 76, 43, 32].

With this background, we attempted to learn a 3D scene model from a single 360-degree image. Recently, 360-

degree cameras that can capture the entire field of view in a single shot have become easily accessible, and significant amounts of 360-degree image data are available through social media and public datasets. Learning NeRF from a single 360-degree image is advantageous; that is, we do not need to align the shooting conditions between images or know the relative positions between images. This is because we use only one image that contains massive omnidirectional information. OmniNeRF [29] is a prior study of this approach; however, it relies only on the neighborhood interpolation ability of the multi-layer perceptron to complete the missing regions caused by occlusion and zooming. This leads to artifacts, and the image quality is significantly reduced when moving away from the camera position of the input image.

In contrast, the technology of completing the missing regions of 2D images (i.e., inpainting or image completion) has been studied for a long time. Recent learning-based approaches such as generative adversary networks (GANs) [22], variational autoencoders (VAEs) [35, 56], and diffusion models [61, 28] have made enabled the generation of semantically high-quality images. In addition, 360-degree image completion has been well-researched [66, 1, 23, 24, 3, 25], and high-quality image completion is possible over the entire field of view. However, 2D image completions generally do not consider the 3D structure; thus, there is no 3D consistency between images completed at multiple camera positions.

In this study, we attempted to synthesize plausible novel views with 3D consistency from a single 360-degree image by combining NeRF and image completion using 360-degree images. To maintain 3D consistency, we introduce a method to learn the NeRF model using a subset of completed images that cover the target scene so that the overlap of the completed regions is smaller. Figure 1 illustrates the overview of our method.

The contributions of this study are as follows.

 We propose a method for synthesizing novel views by learning NeRF from a single 360-degree RGB-D image, which improves image quality by employing the 360-degree image completion.

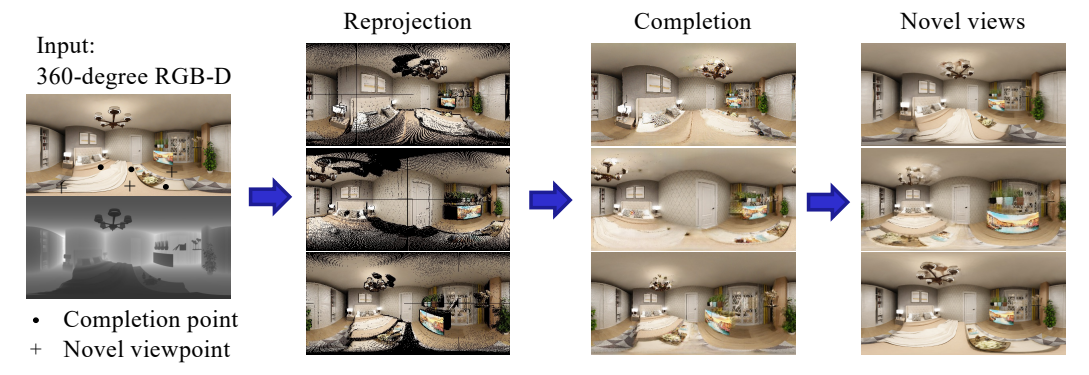


Figure 1. Given only a single 360 RGB-D image, our method can render novel views. The input image is reprojected to 360-degree images at another camera positions, and the missing regions of the reprojected images are completed. A subset of the selected completed images is used to train the NeRF, and novel views are synthesized. Notably, the 360-degree image is represented by the equirectangular projection that maps the longitude of the viewing direction to the horizontal coordinate and the latitude to the vertical coordinate.

- We designed a new architecture that selects a subset of completed images that cover the target scene with less overlap of completed regions to train the NeRF model, allowing us to maintain 3D consistency for novel views.
- We demonstrate that our proposed method can synthesize more plausible views for artificial and real-world data, using new metrics for evaluating the quality of novel views for which no ground truth image exists.

2. Related Work

2.1. Novel view synthesis

Novel view synthesis from a set of captured images has been a consistent challenge in computer vision. Structurefrom-motion [26] is a method that has been employed for a long time for the synthesis of novel view. It can recover point clouds and camera parameters from images of multiple viewpoints. Mesh-based methods have been employed to generate object-centric views [33, 5]; however, it is difficult and impractical to represent an entire scene with a detailed mesh in the real world. The representation method using multi-plane images (MPI) [89, 59] is another way to achieve novel view synthesis in a limited field of view without the need of 3D model. Attal et al. [4] extended the MPI to multi-sphere images for the entire field of view to be rendered; however, it is not suitable for free movement within a scene. Other approaches to view synthesis include image-based rendering [18, 60, 27] and light-field photography [40]; however, they generally require dense capture of the scene.

Recently, rendering techniques using neural networks, which map 3D spatial location to an implicit representation, have been applied to this task [71]. In particular, NeRF [48] can render objects with complex shapes and textures

in a high-quality and photorealistic manner. However, the NeRF requires tens to hundreds of images with known relative positions and the same shooting conditions to be given as input, and such imaging is a large and time-consuming process. Accordingly, various efforts have been made to reduce the number of input images [79, 74, 72, 31, 12], ease the shooting conditions [47, 76, 43, 32], speed up processing [64, 20, 53, 78, 49, 10, 13, 54], and express the entire scene [83, 15, 8, 55, 70, 73].

Among them, OmniNeRF [29] learns an entire scene from a single 360-degree RGB-D image without the need to set relative positions or identify shooting conditions. However, it only relies on the neighborhood interpolation capability of the multi-layer perceptron to complete the missing regions caused by occlusion and zooming, which leads to artifacts. Additionally, the image quality is significantly reduced when moving away from the camera position of the input image. An alternative method to NeRF, pathdreamer [37], synthesizes novel views from a single 360-degree RGB-D image. However, it the method has low 3D consistency in the synthesized views because it is based on 2D image-to-image translation [50].

2.2. Image Completion

Thus far, various image completion technologies for predicting the missing regions of an image have been proposed. Conventionally, many diffusion-based methods [6, 9] diffused the information of the visible regions into the missing regions, and multiple patch-based methods [14, 7] completed the missing regions by matching, copying, and realignment using visible regions. Generative models, which are trained using large-scale datasets, have experienced a significant boost, and the models have been adopted for image completion, with VAE-based methods [87, 51], GAN-based methods [42, 19, 39, 30, 44, 81, 80, 77, 85, 86, 45, 68], autoregressive model-based methods [82, 41, 16], and

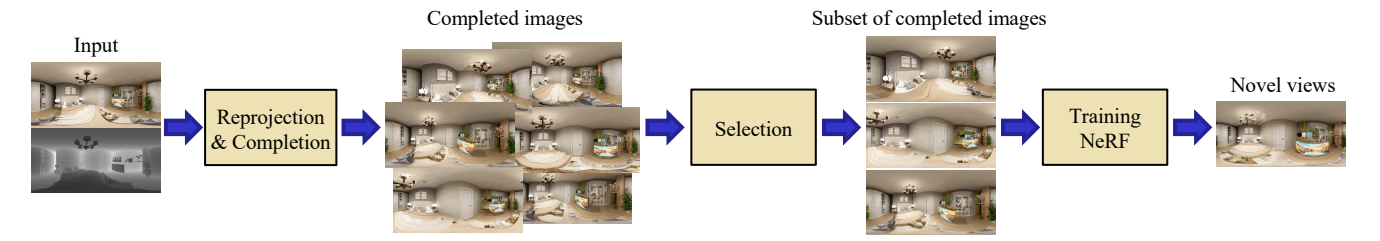


Figure 2. Pipeline of the proposed method. The input image is reprojected and completed as 360-degree images at other camera positions. A subset of the selected completed images is utilized to train the NeRF. Novel views are then synthesized by the trained NeRF.

diffusion model-based methods [46, 57, 58].

360-degree image completion has also been researched. Han et al. [23] proposed an image-inpainting method for spherical structures using a cube map. In [67, 66], a 360-degree image was generated from a set of images captured in multiple directions as an input. Additionally, panoramic three-dimensional structure prediction methods have been proposed [63, 65]. In [21, 62, 2, 1, 24, 3, 25], a 360-degree image was generated from a single normal field of view image. Thus, the technology to complete the missing regions of 360-degree images with high image quality has been developed, and we applied these achievements to the synthesis of novel view.

3. Preliminaries

Here, we present an overview of NeRF and OmniNeRF, which forms the basis of this study. NeRF employs a multi-layer perceptron to construct a function that takes the 3D position $x \in \mathbb{R}^3$ and a unit-norm viewing direction $d \in S^2$ as the input, and outputs density $\sigma \in \mathbb{R}$ and color $c \in \mathbb{R}^3$. Using the approximation method of volume rendering, the density and color on the ray that corresponds to the pixel of the image are integrated to calculate the RGB value. Using images captured from multiple viewpoints, the weights of the MLP are learned to minimize the L2 error between the observed and predicted RGB values.

OmniNeRF [29] generates multiple images at virtual camera positions from a single 360-degree RGB-D image and then utilizes these images to train NeRF. A set of 3D points was generated from the given RGB-D panorama and then the 3D points are reprojected into multiple omnidirectional images that correspond to different virtual camera locations. When reprojecting the 3D points onto the virtual camera spheres, their sparsity of the 3D points causes the back part of the object, which is not originally visible to see through. To address this challenge, a median filter was applied to the depth map to mitigate the sparsity.

4. Proposed Method

Here, we describe our proposed method that learns the NeRF model and synthesizes novel views from a single 360-degree RGB-D image. Figure 2 illustrates the training pipeline of the proposed method. The input image is first reprojected onto 360-degree RGB images of the virtual camera positions, and the missing regions are completed. To maintain 3D consistency, a subset of completed images with less overlap of completed regions is selected. The subset selection is equivalent to the maximum weight independent set problem (MWISP) [52], which is solved using simulated annealing (SA) [36]. The input data to train NeRF includes the selected completed images along with RGB data of the input image and its reprojected image. The NeRF is trained to minimize L2 loss of the synthesized and inputed images.

4.1. Reprojection and completion

First, the input image is reprojected onto 360-degree RGB images of the virtual camera positions. This reprojection adopts the same approach as OmniNeRF, as described in Section 3. The reprojected image has missing regions owing to occlusion and zooming, as illustrated in Fig. 1. We complete the missing regions using OmniDreamer [24], which is an advanced 360 degree image completion method based on VQ-GAN [17]. OmniDreamer was trained from scratch for this purpose; the details of training configurations are described in the Supplemental Material.

4.2. Selection of completion positions

Because image completion is processed in the 360-degree field of view from a single point of view, the consistency between images observed from different positions cannot be guaranteed. Therefore, a set of images for training the NeRF is adaptively selected from the completed images. It is not easy to determine the combination of the completed images that is 3D consistent. We can determine 3D consistency as a result of training NeRF; however, it takes long to train NeRF once, and it is practically difficult to try all combinations. Therefore, we propose a method for selecting a subset of completed images that cover the target scene; thus, the overlap of the completed regions is smaller in the preliminary stages of training NeRF.

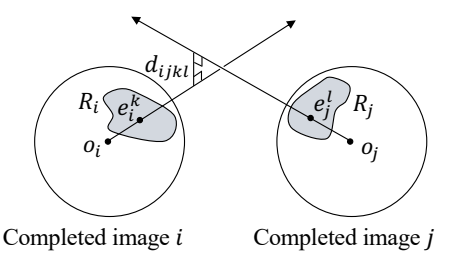


Figure 3. Determination of collision between two rays.

4.2.1 Formulation as optimization problem

Assuming that there are N completed images, we introduce variable $z_i \in \{0,1\}$ that takes 1 if i-th complete image is selected and 0 if not. Let $r_{ij} \in \mathbb{R}$ be the degree of overlap of the completed regions in completed images i and j (Section 4.2.2), R_i is a set of rays corresponding to the completed regions in the i-th complete image, and $|R_i|$ is the number of elements in R_i . We formulate the problem of selecting a subset of completed images for training NeRF as follows:

$$\text{maximize}_{\{z_i\}_{i=1}^N} : \sum_{i=1}^N |R_i| z_i \tag{1}$$

subject to :
$$r_{ij} < C \ (1 \le i < j \le N)$$
 (2)

where C is the threshold parameter that determines overlaps. This optimization problem is equivalent to MWISP. As MWISP is known to be an NP-hard problem [52], we employ SA [36] as the optimization method to obtain a suboptimal solution in practical time. The details of the optimization method are described in the Supplemental Material.

4.2.2 Degree of overlap

We formulated the degree of overlap r_{ij} between i-th and j-th completed images. Determining the overlap between completed regions of different images requires training NeRF, which is time-consuming. Therefore, an assumption is made on the collision probability between rays in the completed region, from which the degree of overlap is estimated.

As shown in Fig. 3, the projection center i-th completed image is described as $o_i \in \mathbb{R}^3$, and the direction of the k-th ray in R_i is describe as $e_i^k \in S^2$. We assume that the probability that rays (o_i, e_i^k) and (o_j, e_j^l) reflect the same location on the surface is as follows:

$$P_{ijkl} = \beta \exp\left(-\frac{d_{ijkl}^2}{2\sigma^2}\right) \exp\left(\kappa \langle e_i^k, e_j^l \rangle\right)$$
 (3)

where β , σ and κ are hyper-parameters, $\langle \cdot, \cdot \rangle$ is inner product, and d_{ijkl} is the minimum distance between rays (o_i, e_i^k)

and (o_j, e_j^l) as follows:

$$d_{ijkl} = \frac{\langle e_i^k \times e_j^l, o_i - o_j \rangle}{||e_i^k \times e_j^l||}.$$
 (4)

Eq. (3) represents that the co-located reflection probability of the rays is expressed as a Gaussian distribution for the distance between the rays and a von Mises-Fisher distribution for the direction of the rays, which are the standard distributions for distances and angles. Using probability P_{ijkl} , the degree of overlap r_{ij} is defined as

$$r_{ij} = \sum_{k \in R_i} \sum_{l \in R_j} P_{ijkl}.$$
 (5)

To speed up the above calculation, a smaller number of pixels are used as R_i , randomly sampled from the completed regions.

4.3. Training NeRF

The model of NeRF is trained using the selected subset of completed images as the input. Although any NeRF model can be used, we employ Instant NGP [49] for fast rendering in this study.

5. Experimental Results

Quantitative and qualitative experiments were conducted to verify the effectiveness of the proposed method for both synthetic and real-world datasets.

5.1. Dataset

5.1.1 Structured3D

Structured3D dataset [88] contains 3,500 synthetic departments (scenes) with 185,985 photorealistic panoramic renderings. As the original virtual environment is not publicly accessible, we utilized the rendered panoramas directly. The data were divided into 3,100 scenes for training, and 400 scenes for testing.

5.1.2 Matterport3D

Matterport3D dataset [11] is a large-scale indoor real-world 360 dataset, which was captured by Matterport's Pro 3D camera in 90 furnished houses (scenes). The dataset provides 10,800 RGB-D panorama images, and the RGB-D signals near the polar region are missing. The data were divided into 71 scenes for training and 19 scenes for testing.

5.2. Implementation Details

We trained the NeRF model using the Adam optimizer [34] while exponentially decreasing the learning rate from

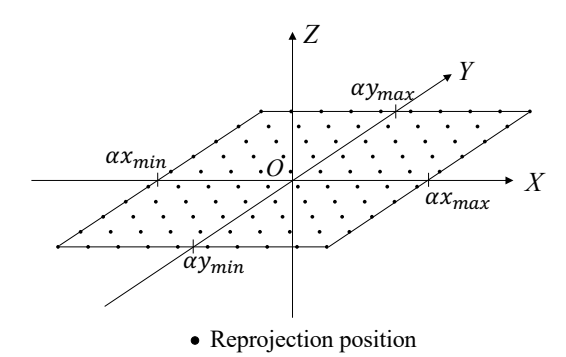


Figure 4. Settings of the reprojection and completion points. The origin O is the camera position of the input image, and the Z-axis is parallel to the direction of gravity and orthogonal to the XY-axis. The reprojection and completion positions are taken at 10×10 grid points by equally dividing interval $[\alpha x_{\min}, \alpha x_{\max}]$ on the x-axis and interval $[\alpha y_{\min}, \alpha y_{\max}]$ on the y-axis, where $\alpha = 0.6$ and $x_{\min}, x_{\max}, y_{\min}, y_{\max}$ are the boundary point of the depth of the input image.

 5.0×10^{-4} to 5.0×10^{-5} . The NeRF model was trained with 200,000 iterations for each experiment with a batch size of 1,400. We set the number of sampling N_c = 64 and N_f = 128 for the coarse and refined networks, respectively. The network structures of NeRF were identical to those of Instant NGP [49]. Learning one scene took approximately 4 hours on an NVIDIA Tesla V100 GPU. The image completion networks were trained on training data, whereas NeRF was trained on test data, according to the division defined in section 5.1. The input images, completed images, and novel views were in equirectangular projection format with a resolution of $1,024\times512$.

As shown in Fig. 4, the reprojection and completion positions are taken at 10×10 grid points by equally dividing the interval $[\alpha x_{\min}, \alpha x_{\max}]$ on the x-axis and the interval $[\alpha y_{\min}, \alpha y_{\max}]$ on the y-axis, where $\alpha = 0.6$ and $x_{\min}, x_{\max}, y_{\min}, y_{\max}$ are the boundary point of the depth of the input image.

For the selection of completion positions, the hyperparameters of P_{ijkl} are set as $\beta=1.0$, $\sigma=0.01$ and $\kappa=1.0$, overlap threshold C is set to 4.0×10^4 , and the sampling rate of the rays for R_i is set to 0.01.

OmniNeRF [29] was used for comparison, and the NeRF model and training settings are identical to those of the proposed method.

5.3. Qualitaive evaluation

First, we qualitatively validate the novel view synthesis using a single 360-degrees RGB-D image. Figure 5 illustrates examples of synthesized novel views using the proposed method. A plausible view with 3D consistency is synthesized at a position different from the camera position of the input. The depth data in the Matterport3D dataset is

subject to measurement error, which results in some distortion in the synthesized views. In Fig. 6 and Fig. 7, we compare images synthesized using OmniNeRF and the proposed method. OmniNeRF produces artifacts and noise in the occlusion regions and in the area where the resolution has changed, whereas the proposed method produces a plausible image. These results indicate that the Image completion is working effectively. Additional results are available in the Supplementary Material.

5.4. Quantitative evaluation

We quantitatively evaluated each method using the following four evaluation metrics of two types:

Reconstruction evaluation We calculated the peak signal-to-noise ratio (PSNR), SSIM [75], and LPIPS [84] between the synthesized and the input images at the position of input image because there is no ground truth image apart from the input image. We used these metrics to evaluate the performance of the input image reconstruction.

Synthesis evaluation We calculate the negative log likelihood of features (NLLF) in the synthesized image by modeling the feature distribution for the test data with a normal distribution, using the 2048 dimensional values of the last pooling layer of inception-v3 [69] as features. A total of 20,000 perspective images are randomly cropped from the test data, and the mean $\mu_f \in \mathbb{R}^{2048}$ and covariance matrix $\Sigma_f \in \mathbb{R}^{2048 \times 2048}$ of the 2048 dimensional features are calculated. The features $\{x_i \in \mathbb{R}^{2048}\}_{i=1}^M$ are calculated by randomly synthesizing M=2000 perspective projection images from the learned 3D scene, and the NLLF is calculated using the following formula:

$$NLLF = \frac{1}{M} \sum_{i=1}^{M} (x_i - \mu_f)^T \Sigma_f^{-1} (x_i - \mu_f)$$
 (6)

This metric evaluates the plausibility of the synthesized views at different positions from the input image.

Because it takes a reasonable amount of time to train and evaluate, we extracted five images from the test data of the Structure3D and Matterport3D to include a variety of scenes, as shown in Fig. 8. The evaluation results for each image are presented in Table 1. The proposed method outperforms OmniNeRF in terms of the NLLF, which indicates that the proposed method can synthesize plausible views that have features close to the test dataset. This could be because the image completion network trained on the training data generalized image features and it plausibly completed the missing regions in the scene. For PSNR, SSIM, and



Figure 5. Visualization of novel view rendering in the proposed method at the evaluation positions defined in Fig. 4. (a) A sample in the Structure3D dataset. (b) A sample in the Matterport3D dataset. A plausible viewpoint image with 3D consistency is synthesized at a position different from the camera position of the input.



Figure 6. Qualitative comparison of OmniNeRF and the proposed method on the Structure3D dataset. OmniNeRF produces artifacts in occlusion regions such as behind the yellow chair in scene S2 and on the wall in scene S4, whereas the proposed method reduces these artifacts. The backless chair in scene S2 has a collapsed image in OmniNerf owing to changes in the resolution and the viewing angle, whereas the proposed method retains its shape.

LPIPS, the proposed method is inferior to OmniNeRF. This could be because the effect of image completion at other locations affect the rendering at the input image position. However, as shown in Fig. 9, there is no significant visual difference between OmniNeRF and the proposed method for the input image reconstruction. Thus, the proposed method can improve the image quality of the novel views

while keeping the input image reconstruction as much as possible.

5.5. Ablation study

We conduct an ablation study with learning NeRF using all 100 completed images without selection. The results are presented in Table 1. In both datasets, PSNR, SSIM,



Figure 7. Qualitative comparison of each novel view synthesis method on the Matterport3D dataset. The Matterport3D dataset contains missing regions at the top and bottom regions of the input image, and the proposed method completes the missing regions naturally, as in the floor of scenes M3 and M5. The refrigerator and the window in scene M2 have some artifacts in OmniNeRF owing to resolution change; however, the proposed method reduces these artifacts.

Table 1. Quantitative evaluation of each novel view synthesis method on 10 images in Fig. 8. PSNR, SSIM, and LPIPS evaluates the performance of the input image reconstruction, whereas negative log likelihood of features (NLLF) evaluates the plausibility of the synthesized views at different positions from the input image. NLLF is described by dividing by 1000. For each data set and each metric, boldface values indicate the best value and underlined values indicate the second best value.

	Structured3D dataset [88]				Materport3D dataset [11]			
		Rec.		Syn.		Rec.		Syn.
	PSNR↑	SSIM↑	LPIPS↓	NLLF↓	PSNR↑	SSIM↑	LPIPS↓	NLLF↓
OmniNeRF [29]	27.497	0.920	0.167	4.796	28.888	0.872	0.251	4.376
Ours (w/o selection)	23.501	0.789	0.255	4.493	26.431	0.812	0.310	4.629
Ours	<u>26.744</u>	<u>0.891</u>	<u>0.203</u>	<u>4.697</u>	<u>27.764</u>	<u>0.838</u>	<u>0.271</u>	4.275

and LPIPS degraded significantly without image selection. Without image selection, the generated image is prone to blurring owing to the representation of inconsistent input images as shown in Fig. 9. When 3D inconsistent images are used as input for NeRF, average and blurred images are acquired. NLLF improves for the Structured3D dataset and degrades for the Matterport3D dataset. This could be because the Matterport3D dataset has a wide space and a large completion area; therefore, various images are completed,

and the image quality could be degraded owing to inconsistencies in the novel views.

5.6. Limitations

Although the performance of the proposed method is promising, it has several limitations. First, if there are large missing regions that exceed the image completion capabilities, it is difficult to synthesize plausible views. Second, the reprojection process highly depends on the depth accuracy,



Figure 8. Input images used in quantitative evaluation. Images beginning with S are from the Strucutred3D dataset while those beginning with M are from the Matterport3D dataset.

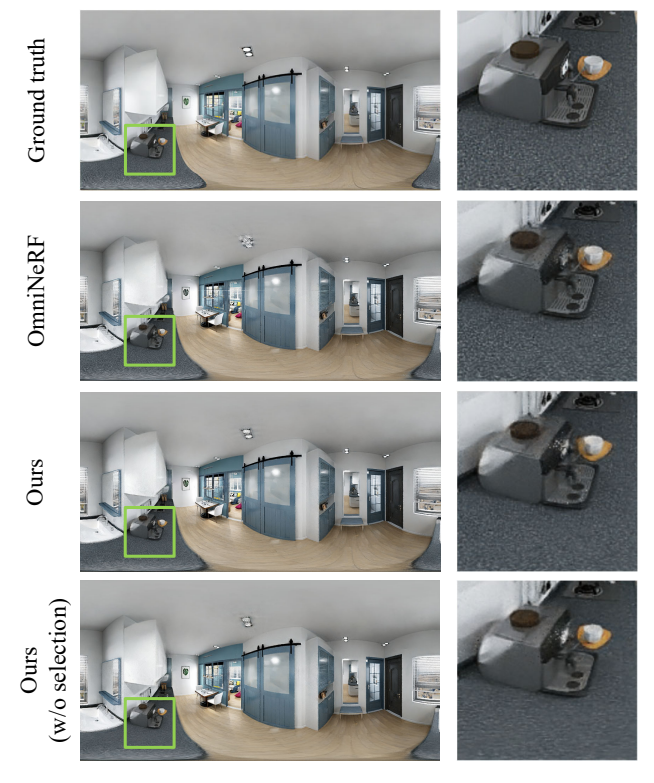


Figure 9. Example of rendering at input image position. The result without selection of the completed images is significantly blurred.

and geometric distortion occurs in the synthesized image when the depth accuracy is low.

6. Conclusions

In this study, we propose a method for synthesizing novel views by learning the NeRF from a single 360-degree RGB-D image. Unlike existing methods [29], the proposed method employed omnidirectional image completion for reprojected images at other camera positions, which were utilized for training the NeRF. Because multiple completed images contain inconsistencies in 3D, we introduced a method to train NeRF using a subset of completed images that cover the target scene with less overlap of completed regions.

The experiments indicated that the proposed method can

synthesize plausible novel views while preserving the features of the scene, both for artificial and real-world data. These results confirm the effectiveness of employing image completion and the selection of a subset of the completed image with consistency for novel view synthesis. Recently, a method for training NeRF from a single 360-degree RGB-D image was proposed, and it used a large vision-language model to maintain consistency of novel viewpoints [38]. Our method has the advantage of being lightweight in processing because it does not use a large vision-language model. Furthermore, since the proposed method can employ any NeRF model, it can be combined with such methods to improve quality.

Acknowledgements

This work was partially supported by JST AIP Acceleration Research JPMJCR20U3, Moonshot R&D Grant Number JPMJPS2011, CREST Grant Number JPMJCR2015, JSPS KAKENHI Grant Number JP19H01115, JP20H05556 and Basic Research Grant (Super AI) of Institute for AI and Beyond of the University of Tokyo.

References

- [1] Naofumi Akimoto and Yoshimitsu Aoki. Image completion of 360-degree images by cgan with residual multi-scale dilated convolution. *IIEEJ Trans. Image Electronics and Vis. Comput.*, 8(1):35–43, 2020. 1, 3
- [2] Naofumi Akimoto, Seito Kasai, Masaki Hayashi, and Yoshimitsu Aoki. 360-degree image completion by twostage conditionalgans. In *Proc. IEEE Int. Conf. Image Pro*cessing, pages 4704–4708, 2019. 3
- [3] Naofumi Akimoto, Yuhi Matsuo, and Yoshimitsu Aoki. Diverse plausible 360-degree image outpainting for efficient 3dcg background creation. In *Proc. IEEE Conf. Comput. Vis. Pattern Recognit.*, pages 11441–11450, 2022. 1, 3, 12
- [4] Benjamin Attal, Selena Ling, Aaron Gokaslan, Christian Richardt, and James Tompkin. Matryodshka: Real-time 6dof video view synthesis using multi-sphere images. In *Europ. Conf. Comput. Vis.*, 2020. 2
- [5] Abhishek Badki, Orazio Gallo, Jan Kautz, and Pradeep Sen. Meshlet priors for 3d mesh reconstruction. In *Proc. IEEE Conf. Comput. Vis. Pattern Recognit.*, page 2846–2855, 2020.
- [6] Coloma Ballester, Marcelo Bertalmio, Vicent Caselles, Guillermo Sapiro, and Joan Verdera. Filling-in by joint interpolation of vector fields and gray levels. *IEEE Trans. Image Processing*, 10(8):1200–1211, 2001. 2
- [7] Connelly Barnes, Eli Shechtman, Adam Finkelstein, and Dan B Goldman. Patchmatch: A randomized correspondence algorithm for structural image editing. ACM Trans. Graph., 28(3), 2009.
- [8] onathan T. Barron, Ben Mildenhall, Dor Verbin, Pratul P. Srinivasan, and Peter Hedman. Mip-nerf 360: Unbounded anti-aliased neural radiance fields. arXiv:2111.12077, 2021.

- [9] Marcelo Bertalmio, Guillermo Sapiro, Vincent Caselles, and Coloma Ballester. Image inpainting. In *Proc. Conf. Comput. Graph. Interact. Techniq.*, pages 417–424, 2000. 2
- [10] Eric R. Chan, Connor Z. Lin, Matthew A. Chan, Koki Nagano, Boxiao Pan, Shalini De Mello, Orazio Gallo, Leonidas Guibas, Jonathan Tremblay, Sameh Khamis, Tero Karras, and Gordon Wetzstein. Efficient geometry-aware 3d generative adversarial networks. arXiv:2112.07945, 2020. 2
- [11] Angel Chang, Angela Dai, Thomas Funkhouser, Maciej Halber, Matthias Nießner, Manolis Savva, Shuran Song, Andy Zeng, and Yinda Zhang. Matterport3d: Learning from rgb-d data in indoor environments. In *Int. Confe. 3D Vis.*, 2017. 4, 7
- [12] Di Chen, Yu Liu, Lianghua Huang, Bin Wang, and Pan Pan. Geoaug: Data augmentation for few-shot nerf with geometry constraints. In Europ. Conf. Comput. Vis., 2022. 2
- [13] Zhiqin Chen, Thomas Funkhouser, Peter Hedman, and Andrea Tagliasacchi. Mobilenerf: Exploiting the polygon rasterization pipeline for efficient neural field rendering on mobile architectures. arXiv:2208.00277, 2022. 2
- [14] Antonio Criminisi, Patrick Perez, and Kentaro Toyama. Object removal by exemplar-based inpainting. In *Proc. IEEE Conf. Comput. Vis. Pattern Recognit.*, pages II–II, 2003.
- [15] Terrance DeVries, Miguel Angel Bautista, Nitish Srivastava, Graham W. Taylor, and Joshua M. Susskind. Unconstrained scene generation with locally conditioned radiance fields. In Proc. IEEE Int. Conf. Comput. Vis., 2021. 2
- [16] Qiaole Dong, Chenjie Cao, and Yanwei Fu. Incremental transformer structure enhanced image inpainting with masking positional encoding. In *Proc. IEEE Conf. Comput. Vis. Pattern Recognit.*, 2022. 2
- [17] Patrick Esser, Robin Rombach, and Bjorn Ommer. Taming transformers for high-resolution image synthesis. In *Proc. IEEE Conf. Comput. Vis. Pattern Recognit.*, 2021. 3
- [18] Christoph Fehn. Depth-image-based rendering (dibr), compression, and transmission for a new approach on 3d-tv. In *Proc. Stereoscopic Displays and Virtual Reality Systems XI*, 2004.
- [19] K. Fukushima and S Miyake. Neocognitron: A new algorithm for pattern recognition tolerant of deformations and shifts in position. *Pattern Recognition*, 15(6):455–469, 1982.
- [20] Stephan J. Garbin, Marek Kowalski, Matthew Johnson, Jamie Shotton, and Julien Valentin. Fastnerf: High-fidelity neural rendering at 200fps. In *International Conference on Computer Vision*, 2021. 2
- [21] Marc-Andre Gardner, Kalyan Sunkavalli, Ersin Yumer, Xi-aohui Shen, Emiliano Gambaretto, Gagne Christian, and Jean-Francois Lalonde. Learning to predict indoor illumination from a single image. ACM Trans. Graph., 9(4), 2017.
- [22] Ian Goodfellow, Jean Pouget-Abadie, Mehdi Mirza, Bing Xu, David Warde-Farley, Sherjil Ozair, Aaronand Courville, and Yoshua Bengio. Generative adversarial nets. In *Proc. Int. Conf. Neural Inf. Process. Syst.*, pages 2672–2680., 2014. 1
- [23] S. W. Han and D. Y. Suh. A 360-degree panoramic image inpainting network using a cube map. CMC-Computers, Materials and Continua, 66(1):213–228, 2021. 1, 3

- [24] Takayuki Hara, Yusuke Mukuta, and Tatsuya Harada. Spherical image generation from a single image by considering scene symmetry. In *Proc. AAAI Conf. Artif. Intell.*, pages 1513–1521, 2021. 1, 3
- [25] Takayuki Hara, Yusuke Mukuta, and Tatsuya Harada. Spherical image generation from a few normal-field-of-view images by considering scene symmetry. *IEEE Transactions on Pattern Analysis and Machine Intelligence*, pages 1–15, 2022. 1, 3
- [26] Richard Hartley and Andrew Zisserman. Multiple view geometry in computer vision. Cambridge university press, 2003, 1, 2
- [27] Peter Hedman, Julien Philip, True Price, Jan-Michael Frahm, George Drettakis, and Gabriel Brostow. Deep blending for free-viewpoint image-based rendering. 37(6):1–15, 2018. 2
- [28] Jonathan Ho, Ajay Jain, and Pieter Abbeel. Denoising diffusion probabilistic models. In *Proc. Int. Conf. Neural Inf. Process. Syst.*, 2020.
- [29] Ching-Yu Hsu, Cheng Sun, and Hwann-Tzong Chen. Moving in a 360 world: Synthesizing panoramic parallaxes from a single panorama. *arXiv:2106.10859*, 2021. 1, 2, 3, 5, 7, 8, 12, 13
- [30] SATOSHI Iizuka, Edgar Simo-Serra, and HIROSHI Ishikawa. Globally and locally consistent image completion. ACM Trans. Graph., 36(4), 2017.
- [31] Ajay Jain, Matthew Tancik, and Pieter Abbeel. Putting nerf on a diet: Semantically consistent few-shot view synthesiss. In *Proc. IEEE Int. Conf. Comput. Vis.*, 2021. 1, 2
- [32] Yoonwoo Jeong, Seokjun Ahn, Christopher Choy, Animashree Anandkumar, Minsu Cho, and Jaesik Park. Selfcalibrating neural radiance fields. In *International Confer*ence on Computer Vision, 2021. 1, 2
- [33] Hiroharu Kato, Yoshitaka Ushiku, and Tatsuya Harada. Neural 3d mesh renderer. In *Proc. IEEE Conf. Comput. Vis. Pattern Recognit.*, page 3907–3916, 2018.
- [34] Diederik P. Kingma and Jimmy Lei Ba. Adam: A method for stochastic optimization. *arXiv:1412.6980*, 2014. 4
- [35] Diederik P Kingma and Max Welling. Auto-encoding variational bayes. *arXiv:1312.6114*, 2013. 1
- [36] Scott Kirkpatrick, C. D. Gelatt Jr, and M. P. Vecchi. Optimization by simulated annealing. *Science*, 220(4598):671–680, 1983. 3, 4, 11
- [37] Jing Yu Koh, Honglak Lee, Yinfei Yang, Jason Baldridge, and Peter Anderson. Pathdreamer: A world model for indoor navigation. In *Proc. IEEE Int. Conf. Comput. Vis.*, 2021. 2
- [38] Shreyas Kulkarni, Peng Yin, and Sebastian Scherer. 360fusionnerf: Panoramic neural radiance fields with joint guidance. arXiv:2209.14265, 2022. 8
- [39] Y. LeCun, B. Boser, J. S. Denker, D. Henderson, R. E. Howard, W. Hubbard, and L. D. Jackel. Backpropagation applied to handwritten zip code recognition. *Neural computation*, 1(4):541–551, 1989.
- [40] Marc Levoy and Pat Hanrahan. Light field rendering. In SIGGRAPH, 2020. 2
- [41] Wenbo Li, Zhe Lin, Kun Zhou, Lu Qi, Yi Wang, and Jiaya Jia. Mat: Mask-aware transformer for large hole image inpainting. In *Proc. IEEE Conf. Comput. Vis. Pattern Recognit.*, 2022. 2

- [42] Yijun Li, Sifei Liu, Jimei Yang, and Ming-Hsuan Yang. Generative face completion. In *Proc. IEEE Conf. Comput. Vis. Pattern Recognit.*, pages 3911–3919, 2017.
- [43] Chen-Hsuan Lin, Wei-Chiu Ma, Antonio Torralba, and Simon Lucey. Barf: Bundle-adjusting neural radiance fields. In *International Conference on Computer Vision*, 2021. 1, 2
- [44] G. Liu, F. A. Reda, K. J. Shih, T. C. Wang, A. Tao, and B. Catanzaro. Image inpainting for irregular holes using partial convolutions. In *Proc. Eur. Conf. Comput. Vis.*, pages 85–100, 2018.
- [45] H. Liu, Z. Wan, W. Huang, Y. Song, X. Han, and J. Liao. Pd-gan: Probabilistic diverse gan for image inpainting. In *Proc. IEEE Conf. Comput. Vis. Pattern Recognit.*, pages 9371–9381, 2021.
- [46] Andreas Lugmayr, Martin Danelljan, Andres Romero, Fisher Yu, Radu Timofte, and Luc Van Gool. Repaint: Inpainting using denoising diffusion probabilistic models. 2022. 3
- [47] Ricardo Martin-Brualla, Noha Radwan, Mehdi S. M. Sajjadi, Jonathan T. Barron, Alexey Dosovitskiy, and Daniel Duckworth. Nerf in the wild: Neural radiance fields for unconstrained photo collections. In *Proc. IEEE Conf. Comput. Vis.* Pattern Recognit., 2021. 1, 2
- [48] Ben Mildenhall, Pratul P. Srinivasan, Matthew Tancik, Jonathan T. Barron, Ravi Ramamoorthi, and Ren Ng. Nerf: Representing scenes as neural radiance fields for view synthesis. In Europ. Conf. Comput. Vis., 2020. 1, 2
- [49] Thomas Müller, Alex Evans, Christoph Schied, and Alexander Keller. Instant neural graphics primitives with a multiresolution hash encoding. arXiv:2201.05989, Jan. 2022. 2, 4, 5
- [50] Taesung Park, Ming-Yu Liu, Ting-Chun Wang, and Jun-Yan Zhu. Semantic image synthesis with spatially-adaptive normalization. In *Proc. IEEE Conf. Comput. Vis. Pattern Recog*nit., 2019. 2
- [51] Jialun Peng, Dong Liu, Songcen Xu, and Houqiang Li. Generating diverse structure for image inpainting with hierarchical vq-vae. In *Proc. IEEE Conf. Comput. Vis. Pattern Recognit.*, pages 10775–10784, 2021. 2
- [52] Wayne Pullan. Optimisation of unweighted/weighted maximum independent sets and minimum vertex covers. *Discrete Optimization*, 6(2):214–219, 2009. 3, 4
- [53] Christian Reiser, Songyou Peng, Yiyi Liao, and Andreas Geiger. Kilonerf: Speeding up neural radiance fields with thousands of tiny mlps. In *Proc. IEEE Int. Conf. Comput.* Vis., Jan. 2021. 2
- [54] Christian Reiser, Richard Szeliski, Dor Verbin, Pratul P. Srinivasan, Ben Mildenhall, Andreas Geiger, Jonathan T. Barron, and Peter Hedman. Merf: Memory-efficient radiance fields for real-time view synthesis in unbounded scenes. arXiv:2208.00277, 2023. 2
- [55] Konstantinos Rematas, Andrew Liu, Pratul P. Srini-vasan, Jonathan T. Barron, Andrea Tagliasacchi, Thomas Funkhouser, and Vittorio Ferrari. Urban radiance fields. arXiv:2111.14643, 2021. 2
- [56] Danilo Jimenez Rezende, Shakir Mohamed, and Daan Wierstra. Stochastic backpropagation and approximate inference in deep generative models. In *Proc. Int. Conf. Mach. Learn.*, pages 1278–1286, 2014. 1

- [57] Robin Rombach, Andreas Blattmann, Dominik Lorenz, Patrick Esser, and Björn Ommer. High-resolution image synthesis with latent diffusion models. 2022. 3
- [58] Chitwan Saharia, William Chan, Huiwen Chang, Chris Lee, Jonathan Ho, Tim Salimans, David Fleet, and Mohammad Norouzi. Palette: Image-to-image diffusion models. In SIG-GRAPH, 2022. 3
- [59] Meng-Li Shih, Shih-Yang Su, Johannes Kopf, and Jia-Bin Huang. 3d photography using context-aware layered depth inpainting. In Proc. IEEE Conf. Comput. Vis. Pattern Recognit., 2020. 2
- [60] Heung-Yeung Shum, Shing-Chow Chan, and Sing Bing Kang. *Image-based rendering*. Springer Science and Business Media, 2008. 1, 2
- [61] Jascha Sohl-Dickstein, Eric A. Weiss, Niru Maheswaranathan, and Surya Ganguli. Deep unsupervised learning using nonequilibrium thermodynamicss. In *Proc. Int. Conf. Mach. Learn.*, 2015.
- [62] Shuran Song and Thomas Funkhouser. Neural illumination: Lighting prediction for indoor environmentsk. In Proc. IEEE Conf. Comput. Vis. Pattern Recognit., pages 6918–6926, 2019. 3
- [63] Shuran Song, Andy Zeng, Angel X. Chang, Manolis Savva, Silvio Savarese, and Thomas Funkhouser. Im2pano3d: Extrapolating 360° structure and semantics beyond the field of view. In *Proc. IEEE Conf. Comput. Vis. Pattern Recognit.*, pages 3847–3856, 2018. 3
- [64] Weiping Song, Chence Shi, Zhiping Xiao, Zhijian Duan, Yewen Xu, Ming Zhang, and Jian Tang. Autoint: Automatic feature interaction learning via self-attentive neural networks. In Proc. IEEE Conf. Comput. Vis. Pattern Recognit., 2021. 2
- [65] Pratul P. Srinivasan, Ben Mildenhall, Matthew Tancik, Jonathan T. Barron, Richard Tucker, and Noah Snavely. Lighthouse: Predicting lighting volumes for spatiallycoherent illumination. In Proc. IEEE Conf. Comput. Vis. Pattern Recognit., pages 8080–8089, 2020. 3
- [66] Julius Surya Sumantri and In Kyu Park. 360 panorama synthesis from a sparse set of images on a low-power device. IEEE Trans. on Comput. Imaging, 6:1179–1193, 2020. 1, 3
- [67] Julius Surya Sumantri and In Kyu Park. 360 panorama synthesis from a sparse set of images with unknown fov. In *IEEE Winter Conf. Applications of Comput. Vis.*, pages 2386–2395, 2020. 3
- [68] Roman Suvorov, Elizaveta Logacheva, Anton Mashikhin, Anastasia Remizova, Arsenii Ashukha, Aleksei Silvestrov, Naejin Kong, Harshith Goka, Kiwoong Park, and Victor Lempitsky. Resolution-robust large mask inpainting with fourier convolutions. In *IEEE Winter Conf. Applications of Comput. Vis.*, 2022. 2
- [69] Christian Szegedy, Vincent Vanhoucke, Sergey Ioffe, Jonathon Shlens, and Zbigniew Wojna. Rethinking the inception architecture for computer vision. In *Proc. IEEE Conf. Comput. Vis. Pattern Recognit.*, 2016. 5
- [70] Matthew Tancik, Vincent Casser, Xinchen Yan, Sabeek Pradhan, Ben Mildenhall, Pratul P. Srinivasan, Jonathan T. Barron, and Henrik Kretzschmar. Block-nerf: Scalable large scene neural view synthesis. arXiv:2202.05263, 2022. 2

- [71] Ayush Tewari, Theobalt Christian, Dan B Goldman, Eli Shechtman, Gordon Wetzstein, Jason Saragih, Jun-Yan Zhu, Justus Thies, Kalyan Sunkavalli, Maneesh Agrawala, Matthias Niessner, Michael Zollhofer, Ohad Fried, Ricardo Martin Brualla, Rohit Kumar Pandey, Sean Fanello, Stephen Lombardi, Tomas Simon, and Vincent Sitzmann. State of the art on neural rendering. Computer Graphics Forum, 2020. 2
- [72] Alex Trevithick and Bo Yang. Grf: Learning a general radiance field for 3d scene representation and rendering. In International Conference on Computer Vision, 2021. 1, 2
- [73] Haithem Turki, Deva Ramanan, and Mahadev Satyanarayanan. Mega-nerf: Scalable construction of large-scale nerfs for virtual fly-throughs. In *Proc. IEEE Conf. Comput. Vis. Pattern Recognit.*, 2022. 2
- [74] Qianqian Wang, Zhicheng Wang, Kyle Genova, Pratul Srinivasan, Howard Zhou, Jonathan T. Barron, Ricardo Martin-Brualla, Noah Snavely, and Thomas Funkhouser. Ibrnet: Learning multi-view image-based rendering. In *Proc. IEEE Conf. Comput. Vis. Pattern Recognit.*, 2021. 1, 2
- [75] Zhou Wang, Alan C. Bovik, Hamid R. Sheikh, and Eero P. Simoncelli. Image quality assessment: from error visibility to structural similarity. *IEEE Trans. Image Process*, 13(4):600–612, 2004. 5
- [76] Zirui Wang, Shangzhe Wu, Weidi Xie, Min Chen, and Victor Adrian Prisacariu. Nerf—: Neural radiance fields without known camera parameters. arXiv:2102.07064, 2021. 1, 2
- [77] Z. Yan, X. Li, M. Li, W. Zuo, and S. Shan. Shift-net: Image inpainting via deep feature rearrangement. In *Proc. Eur. Conf. Comput. Vis.*, pages 1–17, 2018. 2
- [78] Alex Yu, Ruilong Li, Matthew Tancik, Hao Li, Ren Ng, and Angjoo Kanazawa. Plenoctrees for real-time rendering of neural radiance fields. In *International Conference on Com*puter Vision, 2021. 2
- [79] Alex Yu, Vickie Ye, Matthew Tancik, and Angjoo Kanazawa. Pixelnerf: Neural radiance fields from one or few images. In Proc. IEEE Conf. Comput. Vis. Pattern Recognit., 2021. 1, 2
- [80] J. Yu, Z. Lin, J. Yang, X. Shen, X. Lu, and T. S. Huang. Generative image inpainting with contextual attention. in proceedings of the ieee conference on computer vision and pattern recognition. In *Proc. IEEE Conf. Comput. Vis. Pattern Recognit.*, pages 5505–5514, 2018.
- [81] J. Yu, Z. Lin, J. Yang, X. Shen, X. Lu, and T. S. Huang. Free-form image inpainting with gated convolution. In *Proc. IEEE Int. Conf. Comput. Vis.*, pages 4471–4480, 2019.
- [82] Yingchen Yu, Fangneng Zhan, Rongliang Wu, Jianxiong Pan, Kaiwen Cui, Shijian Lu, Feiying Ma, Xuansong Xie, and Chunyan Miao. Diverse image inpainting with bidirectional and autoregressive transformers. In *Proc. ACM Int. Conf. on Multimedia*, 2021. 2
- [83] Kai Zhang, Gernot Riegler, Noah Snavely, and Vladlen Koltun. Nerf++: Analyzing and improving neural radiance fields. *arXiv*:2010.07492, 2020. 2
- [84] Richard Zhang, Phillip Isola, Alexei A. Efros, Eli Shechtman, and Oliver Wang. The unreasonable effectiveness of deep features as a perceptual metric. In *Proc. IEEE Conf. Comput. Vis. Pattern Recognit.*, 2018. 5

- [85] Lei Zhao, Qihang Mo, Sihuan Lin, Zhizhong Wang, Zhiwen Zuo, Haibo Chen, Wei Xing, and Dongming Lu. Uctgan: Diverse image inpainting based on unsupervised cross-space translation. In *Proc. IEEE Conf. Comput. Vis. Pattern Recognit.*, pages 5741–5750, 2020. 2
- [86] S. Zhao, J. Cui, Y. Sheng, Y. Dong, X. Liang, E. I. Chang, and Y. Xu. Large scale image completion via co-modulated generative adversarial networks. In *Proc. Int. Conf. Learn. Representations*, 2021. 2
- [87] Chuanxia Zheng, Tat-Jen Cham, and Jianfei Cai. Pluralistic image completion. In *Proc. IEEE Conf. Comput. Vis. Pattern Recognit.*, pages 1438–1447, 2020.
- [88] Jia Zheng, Junfei Zhang, Jing Li, Rui Tang, Shenghua Gao, and Zihan Zhou. Structured3d: A large photo-realistic dataset for structured 3d modeling. In *Europ. Conf. Com*put. Vis., 2020. 4, 7
- [89] Tinghui Zhou, Richard Tucker, John Flynn, Graham Fyffe, and Noah Snavely. Stereo magnification: Learning view synthesis using multiplane images. In ACM Trans. Graph, 2018.
 2

A. Optimization method for complete images selection

A.1. Algorithm

The optimization problem for selecting a subset of the completed images formulated in Eq. (1) is solved through SA [36]. SA does not only proceed with the search in the direction of higher values of the evaluation function, but also adopts a solution with a specific probability even when the evaluation value becomes worse. The probability of selecting a modified solution is controlled by the temperature parameter T. In the early stages of the search, the temperature is high and a large area is explored, while at the end of the search, the temperature is low and local search is approached. This allows finding a global suboptimal solution without falling into a local solution.

Using the camera pose of the completes images and the positions of the completed regions as input, the algorithm outputs a subset of the completed images to be used for training NeRF. Fig. 10 shows the optimization process flow, which is described below.

- **Step 1:** We calculate the degree of overlap between the completed images using the camera pose of the completes images and the positions of the completed regions according to Eq. (3), (4) and (5).
- **Step 2:** The initial solution is changed K=10 times and optimization by SA is performed; if it is repeated K times, the process is terminated and the best solution in the search is outputted; otherwise, proceed to the next step.
- **Step 3:** Initialize the SA parameters and solution. The temperature T is set to 1.0×10^3 , and the temperature attenuation factor η is set to 0.9995. A randomly selected one completed image is set as the initial solution, and the

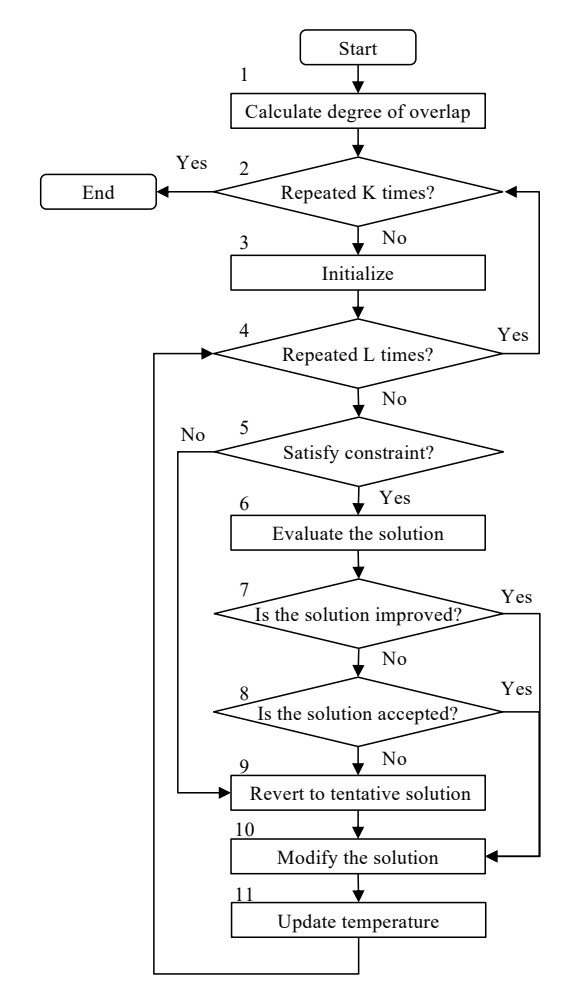


Figure 10. The optimization process flow for the complete images selection

one that includes no completed images is set as the tentative solution.

Step 4: L=20,000 iterations were used to terminate one search. if it is repeated L times, go to Step 2; otherwise, proceed to the next step.

Step 5: Determine if the current solution, a subset of the completed images, has no overlap based on the constraint Eq. (2). If the constraints are satisfied, proceed to the next step; otherwise, go to Step 9.

Step 6: Calculate the value of the evaluation function in Eq. (1), i.e., the number of rays in the completed area of the completed images selected as the solution.

Step 7: If the current solution evaluation value is higher than the tentative solution evaluation value, the tentative solution is updated with the current solution and go to Step 10. Otherwise, go to the next step.

Step 8: Accept the current solution with probability $\exp(d/T)$, where d is the evaluation value of the current solution minus the tentative evaluation value. If the current

solution is accepted, the tentative solution is updated with the current solution and go to Step 10. Otherwise, go to the next step.

Step 9: Revert the current solution to the tentative solution.

Step 10: Modify the current solution. We randomly selects a new completed image to add to the solution with 10% probability, randomly deletes a completed image in the current solution with 10% probability, and replaces completed images in the current solution with the completed images in the neighborhood with 80% probability. For the replacement of completed images in the neighborhood, the completed images have the indices of $\{1,2,\cdots,10\} \times \{1,2,\cdots,10\}$ grid, and the random numbers sampled from the standard normal distribution are added to the indices and rounded to integer values.

Step 11: The temperature T is updated as $T \leftarrow \eta T$, and return to step4.

A.2. Processing time

We measured the processing times of the above optimization algorithms on the Tesla V100. Ten trials were performed, and the average processing time was 222.1 sec, standard deviation 148.4 sec, and maximum 488.3 sec. The variation in processing time is due to the fact that the computational complexity is on the order of squared for the number of completed images selected as the solution.

A.3. Selected completed images

Figure 11 shows an example of the content and location of the completed images selected to train NeRF. Notably, although not indicated in this figure, 100 non-completed reprojection images were also utilized to train NeRF, as in OmniNeRF [29]. From this figure, it can be seen that the completed images are selected to be widely distributed in space to cover the occlusion region. Many images are selected near the input image position (0, 0), because the completed region is smaller near the input image, resulting in less overlap.

B. Details of Image Completion

B.1. Settings

We utilized OmniDreamer [3] as the image completion network. We trained the network using the training data in section 5.1 and 3,200 randomly generated masks. Default settings in [3] are used for training and model hyperparameters.

B.2. Completed images

Examples of images in which the missing pixels in the reprojected images are completed by OmniDreamer is shown in Fig. 12.

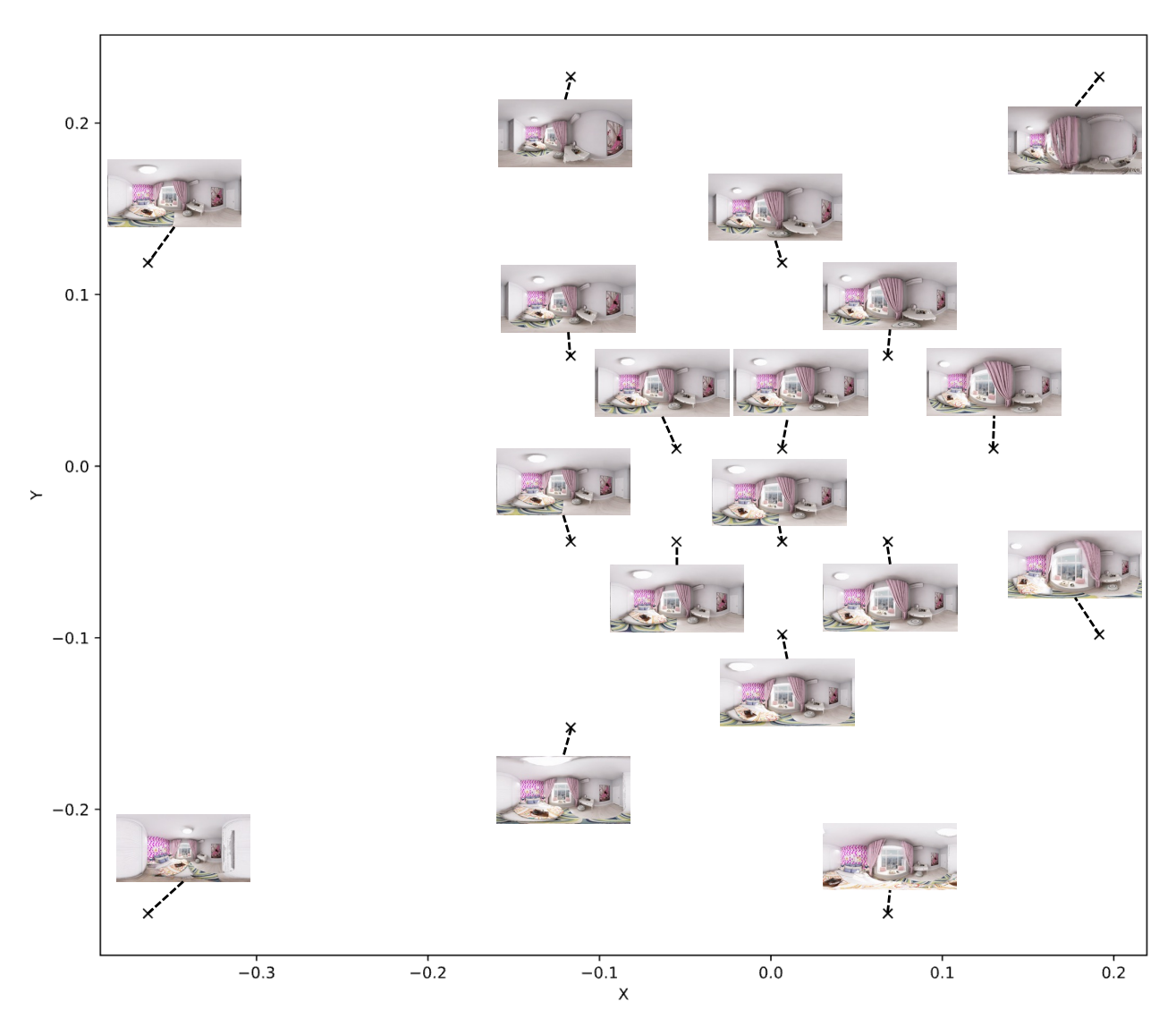


Figure 11. Example of the content and location of the completed images selected to train NeRF. The X- and Y-axis lie on a plane that is orthogonal to gravity axis Z, and the maximum depth in the input image is scaled to 1.0. The each completed image exists on a grid equally divided by 10 points in the x-axis interval [-0.363, 0.192] and y-axis interval [-0.261, 0.227], respectively.

C. Validity of NLLF

We introduced a novel metric, NLLF, for quantitative evaluation of the image quality of novel views. To confirm the validity of this metric, examples of images and NLLF values are shown in Fig. 13. In this figure, NLLF is calculated using 512 perspective images randomly cropped from a single 360-degrees image. The smaller the value of NLLF, the better the perceived image quality appears.

D. Additional Results

D.1. Synthesized novel views

The results of novel view synthesis using OmniNeRF [29] and the proposed method (with and without the completed images selection) in scenes S1, S3, S4, M1, M2, and M4 are illustrated in Fig. 14, 15, 16, 17, 18 and 19. The figures show synthesized novel views in equirectangular and perspective projections with different camera positions.

D.2. Rendering from a free moving camera

Examples of rendering from a freely moving camera are shown in Fig. 20. In the figure, novel views are rendered in perspective projection with a horizontal field of view of 90



Figure 12. Examples of the completed images. Black pixels on the reprojected images are missing pixels due to occlusion or resolution change.

degrees.

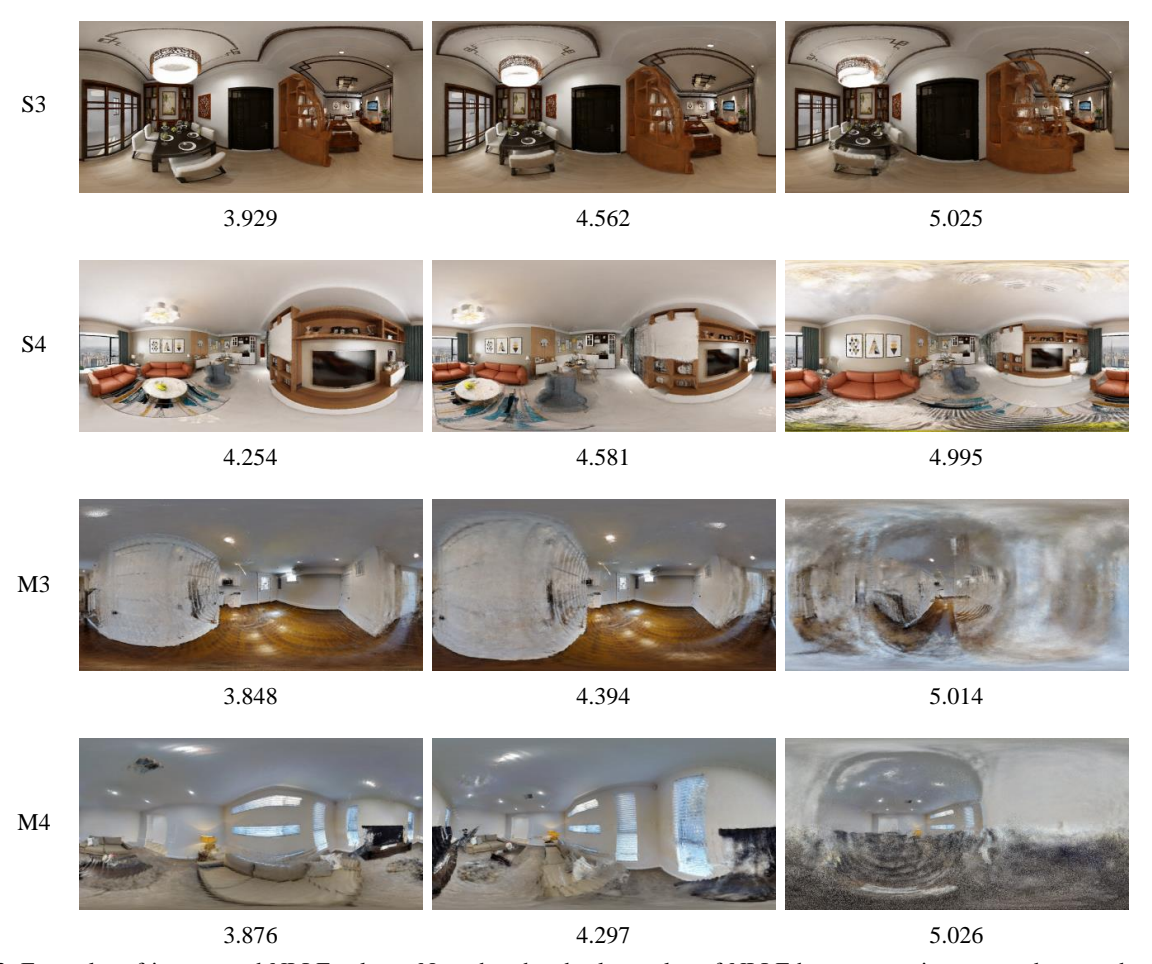


Figure 13. Examples of images and NLLF values. Note that the absolute value of NLLF has no meaning across data sets because the likelihood models are different for Structured3D dataset and Matterport3D dataset.



Figure 14. Novel views synthesized in equirectangular and perspective projections with different camera positions for scenes S1.

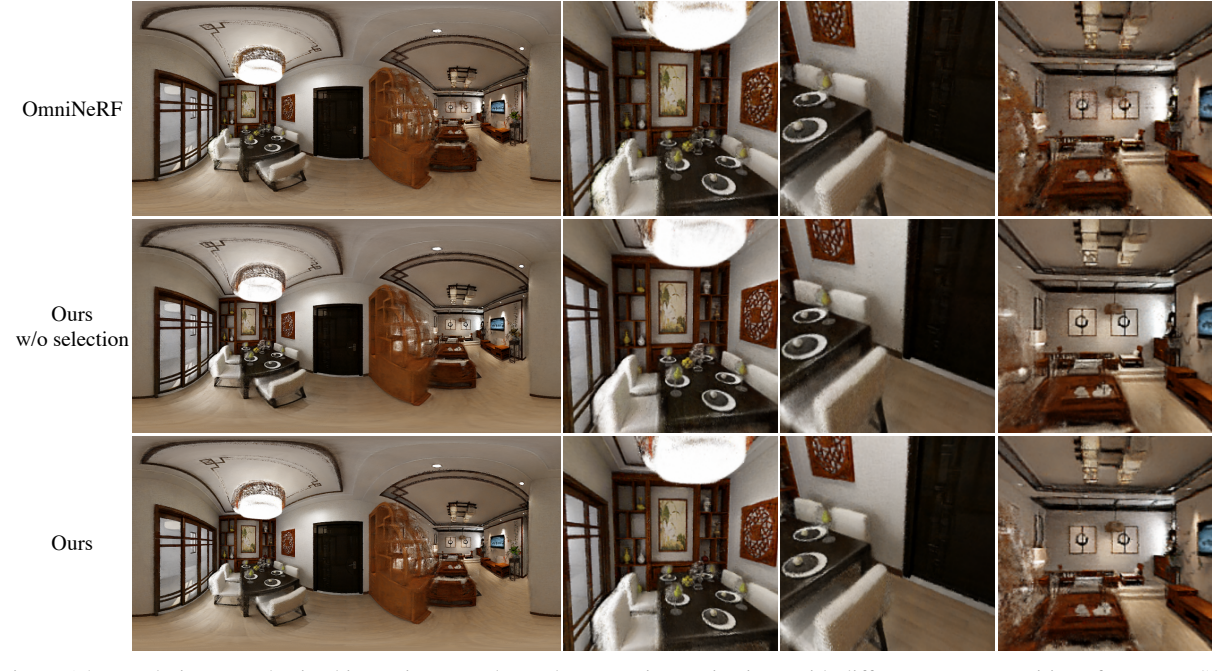


Figure 15. Novel views synthesized in equirectangular and perspective projections with different camera positions for scenes S3.



Figure 16. Novel views synthesized in equirectangular and perspective projections with different camera positions for scenes S4.



Figure 17. Novel views synthesized in equirectangular and perspective projections with different camera positions for scenes M1.



Figure 18. Novel views synthesized in equirectangular and perspective projections with different camera positions for scenes M2.



Figure 19. Novel views synthesized in equirectangular and persptective projections with different camera positions for scenes M4.

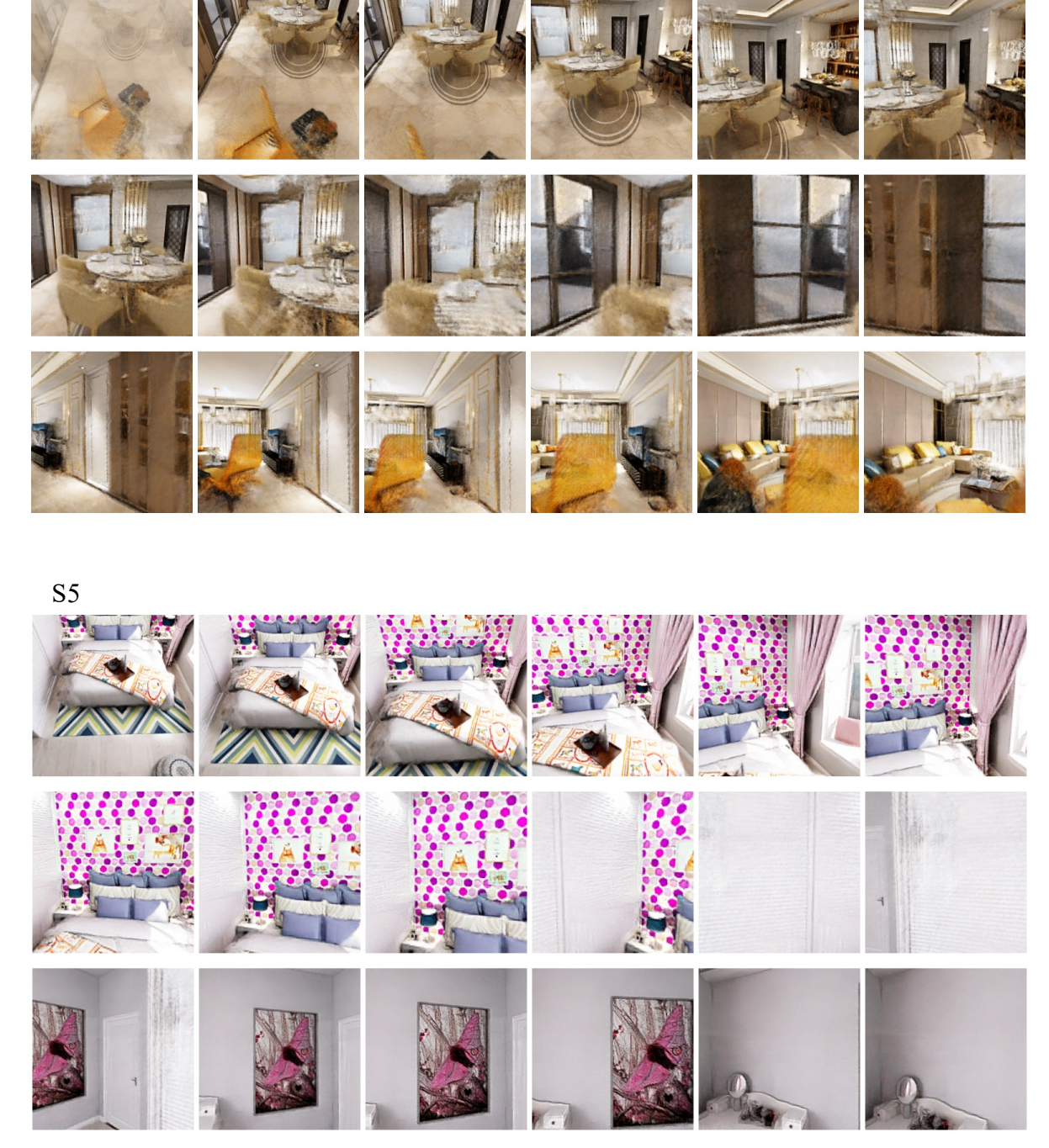


Figure 20. Examples of rendering from a freely moving camera. The novel views are rendered in perspective projection with a horizontal field of view of 90° .